Isotope Engineering in Nanotube Research

Ferenc Simon*

Budapest University of Technology and Economics, Institute of Physics
and Condensed Matter Research Group of the Hungarian Academy of Sciences
H-1521, Budapest P.O.Box 91, Hungary
and
Fakultät für Physik, Universität Wien
Strudlhofgasse 4, A-1090 Wien, Austria

*ferenc.simon@univie.ac.at

Abstract

Single-wall carbon nanotubes (SWCNT) are in the forefront of material sciences due to their compelling structural and electronic properties. In addition to the number of existing and foreseen applications, they display a rich variety of unique fundamental phenomena such as quasi one-dimensional quantum transport, excitonic optical excitations, and correlated electronic states, which we review herein. Several open questions in the field could be addressed using isotope engineering, i.e. a controlled allocation of the less abundant ^{13}C isotope on the nanotubes. The major tool to the isotope engineering of SWCNTs is the ability to encapsulate fullerenes into the hollow inside of the tubes. Upon high temperature annealing, the encapsulated fullerenes form a small diameter inner nanotube. We show that with the use of ^{13}C isotope enriched fullerenes, enrichment of the inner nanotube can be achieved while leaving the host outer tubes and other carbon phases in the sample unaffected. This helps to identify vibrational modes as their vibrational energy changes upon isotope enrichment. The encapsulated ^{13}C allows to trace whether carbon is diffusing along the tube axis during the annealing, which helps to understand the inner tube growth mechanism. Such isotope engineered nanotubes are excellent for nuclear magnetic resonance (NMR) spectroscopy as only nanotubes are enriched and not the inevitably present other carbonaceous phases. Measurement and analysis of the NMR spin lattice relaxation rate allows to identify the correlated state of the SWCNTs as the Tomonaga-Luttinger liquid state.

Contents

Key words Carbon nanotubes Fullerene encapsulation Double-wall carbon nanotubes Isotope engineered nanotubes Raman spectroscopy Magnetic resonance spectroscopy

1 Introduction

The nano-era started with the discovery of carbon nanotubes (CNTs) by Sumio Iijima in 1991 (Iijima 1991). Before 1991, nanoscience and nanotechnology usually meant small clusters of atoms or molecules of seemingly fundamental interest only. The discovery of fullerenes in 1985 (Kroto et al. 1985) revolutionized several fields in chemistry, physics, and also in bio-medical sciences. Fullerenes gave material scientist a fresh look at carbonaceous systems: it suggested that there may exist a number of other forms of carbon which await discovery. The discovery of Iijima fulfilled this expectation and brought the attention to nanosciences, even though discovery of nanotubes had been reported before (Monthioux and Kuznetsov 2006). In fact, he was using the same apparatus which was used for the production of fullerenes. The originally discovered multi-wall CNTs (MWCNTs) were soon followed by the discovery of single-wall CNTs (SWCNTs) (Iijima and Ichihashi 1993, Bethune et al. 1993), which can be grown in similar conditions as the fullerenes and MWCNTs but exclusively in the presence of metal catalysts.

SWCNTs are the one-dimensional allotropes of carbon, completing the list of zero- (the fullerenes (Kroto et al. 1985)), two- (the graphene (Novoselov et al. 2004)), and three-dimensional (graphite and diamond) carbon allotropes. An interesting property of SWCNTs is that all constituent carbons are equivalent and closely sp^2 bound, like in graphite, which provides unique mechanical and transport properties. This, combined with their huge, >1000, aspect ratio (the diameters being 1-20 nm and their lengths over 1 micron), endows them with an enormous application potential and a range of unique and exotic physical properties.

The not exhaustive list of applications includes field-emission displays due to their sharp tips (Obraztsov et al. 2000), cathode emitters for small sized x-ray tubes for medical applications (Yue et al. 2002), reinforcing elements for CNT-metal composites, tips for scanning probe microscopy (Hafner et al. 1999), high current transmitting wires, cables for a future space elevator, elements of nano-transistors (Bachtold et al. 2001), and elements for quantum information processing (Harneit et al. 2002).

However, several fundamental questions need to be answered before the benefits of these novel nanostructures could be fully exploited. Recent theoretical and experimental efforts focused on the understanding of the electronic and optical properties of single-wall carbon nanotubes. It has been long thought that the one-dimensional structure of SWCNTs renders their electronic properties inherently one-dimensional (Hamada et al. 1992, Saito et al. 1998). This was suggested to result in a range of exotic correlated phenomena such as the Tomonaga-Luttinger (TLL) state (Egger and Gogolin 1997),

the Peierls transition (Bohnen et al. 2004, Connétable et al. 2005), ballistic transport, and bound excitons (Kane and Mele 2003, Spataru et al. 2004, Perebeinos et al. 2004). The presence of the TLL state is established (Bockrath et al. 1999, Ishii et al. 2003, Rauf et al. 2004), there is evidence for the ballistic transport properties (Tans et al. 1997) and there is growing experimental evidence for the presence of excitonic effects (Wang et al. 2005, Maultzsch et al. 2005).

Isotope engineering is a useful tool in material science. It can be defined as isotope enrichment of materials, with a control over the isotope allocation. The fundamental property of isotope engineering lies in the fact that to a good approximation (this is also called the Born-Oppenheimer approximation) a different isotope leaves the electronic properties unaffected while changing the energy of the vibrations only. Therefore isotope engineering provides an extra degree of freedom for studies of physical phenomena wherever the energy of vibrations (or phonons in a solid) are involved. Such physical phenomena includes e.g. phonon-mediated superconductivity (Bardeen et al. 1957) and phonon-dominated heat conduction (Capinski et al. 1997). Isotope engineering facilitates the interpretation of vibrational spectra such as e.g. in infrared and Raman spectroscopies.

An additional benefit of isotope engineering is being able to change the nucleus itself. Different nuclei i) have different nuclear spin, I, which allows to perform nuclear magnetic resonance (NMR), ii) allow nuclear reactions with well defined end products when an external irradiation is used. Several stable and most abundant isotopes such as e.g. the ^{16}O and ^{12}C have $I = 0$ which are NMR silent but their isotopes, ^{17}O and ^{13}C, have $I = 1/2$ which make them suitable NMR probes. A particularly compelling use of isotope engineering is the layer selective phosphorus doping of isotope engineered and ready-prepared Si heterostructures by means of neutron irradiation (Meese 1979). A recent proposal suggested the use of isotope engineering to provide the basic architecture for spintronics and quantum computing (Shlimak 2004). In biomedical sciences, isotope engineering is commonly used to allow e.g. molecule site specific NMR experiments and to trace in-vivo reactions with radioactive agents such as tritium, ^{3}H.

The most abundant isotope of carbon is ^{12}C, however 1.1 % of natural carbon is the stable ^{13}C isotope. ^{13}C enriched carbon is available commercially in the form of enriched organic solvents such as ^{13}C-benzene, fullerenes, or graphite. ^{13}C enriched SWCNTs have only been prepared for scientific research. Here, we show how ^{13}C isotope engineering can be used to study the properties of SWCNTs. The examples include the study of SWCNT growth, the vibrational properties including the identification of previously unknown vibrational modes, and the NMR investigations aimed at the understanding of the nature of the correlated ground state in SWCNTs. The review is organised as follows: we describe the fundamentals of the physics of SWCNTs, we describe the applied experimental tools and the synthesis methods for isotope engineering. We finally discuss the knowledge gained using isotope engineering on the vibrational properties and on the correlated ground state in SWCNTs.

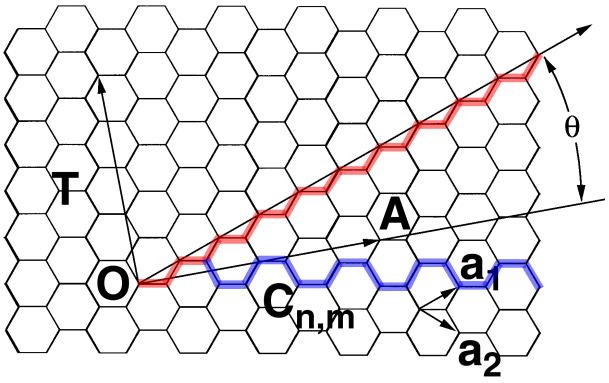

Figure 1: Geometry of a graphene sheet. $\mathbf{a}_1$ and $\mathbf{a}_2$ are the primitive lattice vectors. $\mathbf{A}$ is the vector which joins two carbons which become identical after the rolling-up of a stripe cut out along the vector $\mathbf{T}$. θ is measured between $\mathbf{a}_1$ and $\mathbf{A}$ and is called the chiral angle. The Hamada vectors for an armchair (lower solid curve) and a zig-zag (upper solid curve) are indicated.

2 State-of-the art of single wall carbon nanotube research

2.1 Geometry and electronic properties of SWCNTs

Carbon nanotubes can be represented as rolled up graphene sheets, i.e. single layers of graphite. Depending on the number of coaxial carbon nanotubes, they are usually classified into multi-wall carbon nanotubes (MWCNTs) and single-wall carbon nanotubes (SWCNTs). Some general considerations have been clarified in the past 17 years of nanomaterial research related to these structures. MWCNTs are more homogeneous in their physical properties as the large number of coaxial tubes smears out individual tube properties. This makes them suitable candidates for applications where their nanometer size and the conducting properties can be exploited as e.g. nanometer sized wires. In contrast, SWCNT materials are grown as an ensemble of weakly interacting tubes with different diameters. The physical properties of similar diameter SWCNTs can change dramatically as the electronic structure is very sensitive to the rolling-up direction, the so-called chiral vector (Hamada et al. 1992, Saito et al. 1998). We show the geometry of a graphene sheet and the folding/chiral vector in Fig. 1.

The chiral vector is characterized by the (n, m) vector components which denote the direction along which a graphene sheet is rolled up to form a nanotube.

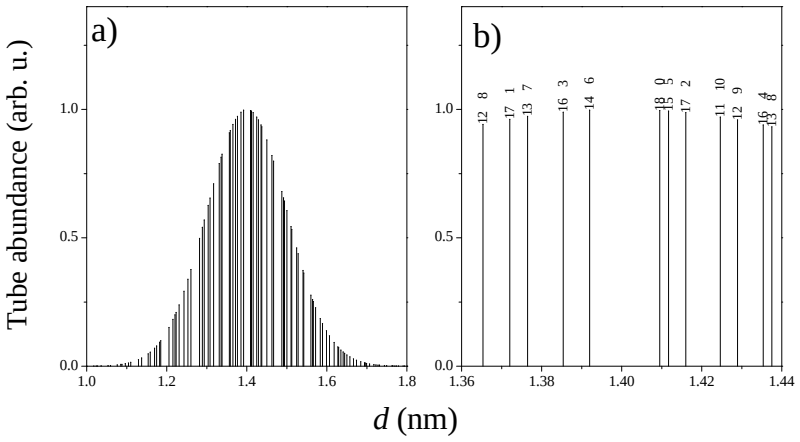

Figure 2: Diameter distribution for a typical SWCNTs (a) and diameter distribution on a magnified scale showing the chiral indices as well (b). Vertical lines represent a geometrically allowed chirality.

The (n, m) indices determine the d diameter of the SWCNTs:

$$d = \frac{a_0\sqrt{n^2 + m^2 + n \cdot m}}{\pi}, \tag{1}$$

where $a_0 = 0.2461$ nm is the length of the C-C bond (Saito et al. 1998). It turned out that for a given sample the diameters of the SWCNTs follow a Gaussian distribution, which is characterized by the mean diameter, d_{mean} and its variance σ. In Fig. 2., we show the diameter distribution for a typical sample with $d_{\text{mean}} = 1.4$ nm and $\sigma = 0.1$ nm. In addition to their local needle-like structure, SWCNTs arrange themselves in a three-dimensional, closely packed hexagonal lattice due to Van der Waals forces, which are the so-called bundles. The tube-wall to tube-wall distance is close to the 3.35 Åfound in graphite (Saito et al. 1998).

The quasi one-dimensional structure of SWCNTs is reflected in their electronic properties: there is a quasi-continuous electron dispersion along the k direction that corresponds to the tube axis and we find discrete states along the other two directions. The SWCNT band-structure can be derived from that of graphene. The latter is a zero band metal where valence and conduction bands touch at the edges of the Brillouin zone at 6 points (the K points). Upon rolling up the graphene sheet in real space, the SWCNT valence and conduction bands can meet at the K points (giving a metallic SWCNTs) or miss each other (making a semiconducting or insulating SWCNT). Simple geometry rules summarize the metallicity versus chiral indices dependence: an SWCNT is metallic if $(n - m)$ mod $3 = 0$ and it is semiconducting if $(n - m)$ mod $3 \neq 0$. These

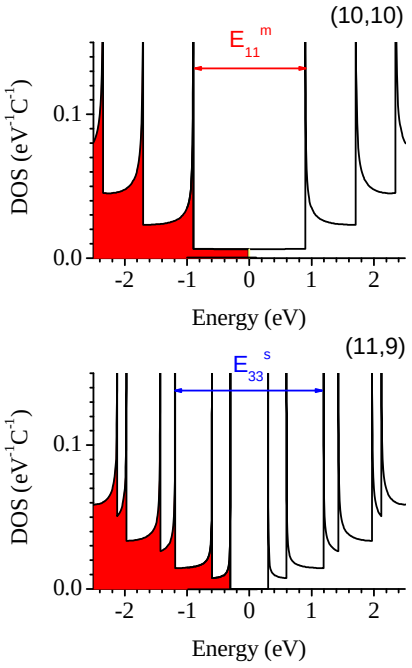

Figure 3: Density of states for the metallic (10,10) and the semiconducting (11,9) SWCNTs near the Fermi energy calculated with the tight-binding model. Filled and open areas indicate filled and empty states. We give as an example the first (E_{11}^m) optical transition for the metallic, and the third optical transition (E_{33}^s) for the semiconducting nanotube.

rules apply to SWCNTs with $d \gtrsim 1.5$ nm as for smaller diameters curvature effects, i.e. deviation of the local bonding from the planar sp^2 arrangement, play an important role (Zólyomi and Kürti 2004). According to the above rules, an SWCNT sample contains bundles with mixed semiconducting and metallic SWCNTs with a 2:1 abundance. Clearly, this property severely limits applicability of the tubes in e.g. nano-electronics, where well defined metallicity is desired.

We find Van Hove singularities in the density of states (DOS) of the SWCNTs due to their quasi one-dimensionality. The singularities are symmetric to the Fermi energy when calculated in the tight-binding (TB) model (Dresselhaus et al. 2001) and we show the DOS for two SWCNTs in Fig. 3 which are representative for the metallic (the 10,10 tube) and for semiconducting (the 11,9 tube) SWCNTs. These tubes have very similar diameters according to Eq. 1., while their electronic property is very different. The Van Hove singularities were first detected using scanning tunneling spectroscopy (Wildör et al. 1998). The selection rules of optical transitions allow transitions between symmetric Van Hove singularity pairs only. The optical transition energies of the metallic and semiconducting SWCNTs are also different. Denoting the optical transitions for metallic (m) and semiconducting (s) SWCNTs with $E_{ii}^{\mathrm{m/s}}$, where ii is the index of the singularity pair, the TB calculation yields (Kataura et al. 1999):

$$E_{ii}^{\mathrm{m}} \approx \mathrm{i} \cdot \frac{0.85 \text{ [eV nm]}}{d \text{ [nm]}}$$
$$E_{ii}^{\mathrm{s}} \approx \mathrm{i} \cdot \frac{2.55 \text{ [eV nm]}}{d \text{ [nm]}} \tag{2}$$

The *tight-binding* result shows that the optical transition energies are inversely proportional to the diameter and that they are very different for metallic and semiconducting tubes. The presence of the Van Hove singularities dominate the optical properties of SWCNTs and have been experimentally confirmed using Raman spectroscopy (Kuzmany et al. 2001, Fantini et al. 2004, Telg et al. 2004) and band-gap fluorescence (Bachilo et al. 2002). More recent "symmetry adapted tight-binding" calculations by Popov (Popov 2004) have refined Eq. 2. and has shown that characteristic deviations arise from the simplest $E_{\mathrm{ii}} \propto 1/d$ rule for tubes in the same "families", i.e. for which $n + 2m = \text{const}$.

As mentioned, the presence of locally mixed semiconducting and metallic nanotubes significantly limits the range of applications. To date, neither the chirality controlled growth nor the selection of SWCNTs with a well defined chiral vector has been performed successfully. Correspondingly, current research is focused on the post-synthesis separation of SWCNTs with a narrow range of chiralities (Chattopadhyay et al. 2003, Krupke et al. 2003, Chen et al. 2003, Zheng et al. 2003) or with separated metallic and semiconducting nanotubes (Arnold et al. 2006). Additionally, methods which yield information that are specific to SWCNTs with different chiralities are important. Examples for the latter are the observation of chirality selective band-gap fluorescence in semiconducting SWCNTs (Bachilo et al. 2002) and chirality assigned resonant Raman scattering (Fantini et al. 2004, Telg et al. 2004).

2.2 Synthesis of SWCNTs

Synthesis methods of SWCNTs share the common ingredient that they all employ a catalyst, unlike the synthesis of MWCNTs or fullerenes. The catalysts are usually transition metal elements (such as Ni, Co, and Fe) and less frequently rare earth elements (e.g. Y). There are two major synthesis methods: one is based on the evaporation of a graphite source and other kinds are the chemical vapor deposition (CVD) methods. Graphite evaporation based methods are the laser ablation (i.e. evaporating a graphitized carbon+catalyst target by a powerful laser) and the arc discharge method (two graphite rods are evaporated by a high current arc in between) which are performed in helium atmosphere. For the CVD methods, carbon source is some small organic molecule such as e.g. ethanol, while t a powder of the catalyst is placed in the reactor which is kept at a few hundred degrees centigrade.

The commonly accepted model of SWCNT growth (Reich et al. 2004) states that the small catalyst particles absorb carbon and form metastable metal-carbides. Upon further absorption, they become saturated with carbon and

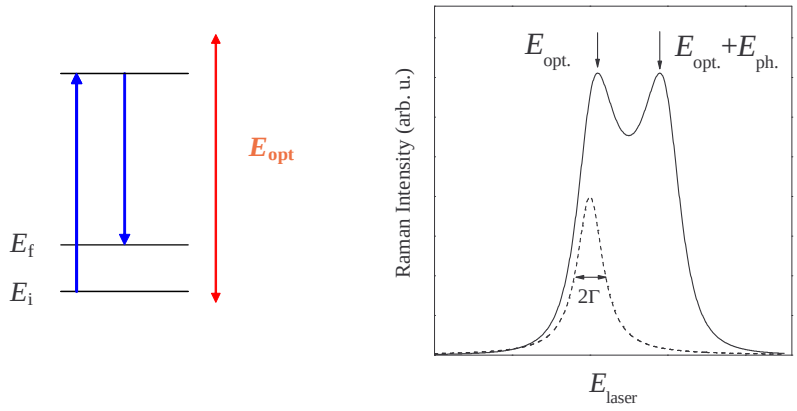

Figure 4: Left panel: Schematics of the Stokes Raman process, E_i and E_f are the initial and final states, respectively. Right panel: schematics of the resonant Raman intensity as a function of the exciting laser energy. Dashed curve indicates the incoming resonant curve alone and the line-width, 2Γ, as defined in the text.

spontaneous growth of SWCNTs starts in a "hedgehog"-like fashion. The end of the nanotubes are closed with caps. As the reaction proceeds, further absorbed carbons continue the growth of the SWCNTs. The SWCNT phase has a larger surface energy compared to the MWCNTs due to the larger curvature. Therefore the effect of the metals is to lower this surface energy thus allowing the formation of SWCNTs. The growth of SWCNTs is essentially a random process with no preferred chirality of a nanotube, however experimental conditions such as the temperature and the type of catalyst selects a nominal diameter (Kataura et al. 1999). This results in the already discussed Gaussian distribution of tube diameters.

2.3 Raman spectroscopy of SWCNTs

We discuss Raman scattering as it is one of the most important experimental methods of the SWCNT resarch. Raman spectroscopy is an inelastic light scattering method. The Raman process involves the absorption and re-emission of light quanta whose energy differs by the energy of an vibration (a true vibrational state for a molecule and an optical phonon for a solid). The process is called correspondingly Stokes or anti-Stokes if a vibration is induced or carried away by the light. The Raman process is of a very low efficiency and laser sources are used to enable efficient discrimination of the inelastically scattered light from the elastically scattered stray-light.

An important property of Raman scattering, which is particularly relevant for SWCNTs, is the so-called resonant Raman enhancement. It turns out that

Raman process can be described by the creation of a short living quasi-particle which carries the energy and momentum of the incoming light. The probability of creation and decay of the quasi-particle according to the Raman process is orders of magnitude enhanced if either the incoming laser energy (the so called incoming resonance) or the outgoing light energy (the so called outgoing resonance) matches an optical transition of the system. This situation is depicted in Fig. 4 and the correspond Raman cross section (or Raman intensity) is given by (Kuzmany 1998):

$$I(E_{\mathrm{l}}) \propto M_{\mathrm{eff}}^{4} \left| \int \frac{\left(E_{\mathrm{l}} - E_{\mathrm{ph}}\right)^{2} \cdot g_{\mathrm{JDS}}(\epsilon) d\epsilon}{\left(E_{\mathrm{l}} - \epsilon - i\Gamma\right)\left(E_{\mathrm{l}} - E_{\mathrm{ph}} - \epsilon - i\Gamma\right)} \right|^{2} \tag{3}$$

where $I(E_{\mathrm{l}})$ is the Raman intensity for a given exciting laser energy, E_{l}. The Raman intensity gives the proportion between the number of incoming and scattered photons for a solid angle of unity. M_{eff} is the effective electron-phonon coupling constant which determines the probability of the quasi-particle creation. E_{ph} is the energy of the investigated vibration or phonon and Γ is the so-called damping parameter and $\Gamma = \hbar/\tau$, where τ is the life-time of the excited quasi-particle. $g_{\mathrm{JDS}}(\epsilon)$ is the strength or density of the optical transition which depends on the occupation of the starting and final states of the optical transitions (the *Joint Density of States*). $g_{\mathrm{JDS}}(\epsilon)$ is directly related to the strength of the Van Hove singularities.

As mentioned, SWCNTs have particularly strong optical transitions due to the Van Hove singularities in the DOS. This means that with a particular choice, Raman spectroscopy can be tuned to particular SWCNT chiralities which are in resonance. This photo-selective property is exploited extensively for the characterization of SWCNT samples with unknown chirality distributions.

The energy difference between the outgoing and incoming light is negative for the Stokes process which is by definition a positive Raman shift. It directly gives the energy of Raman allowed vibrations. In Fig. 5., we show a typical Raman spectrum. We also give the labeling of the most important Raman active modes. As SWCNTs are macro-molecules, their vibrational states can be referred to as both vibrations in the molecular language or as phonons in the solid state physics terminology. The strongest G (or graphitic) mode is related to the tangential motion of carbon, the D mode is related to a non $k \neq 0$ phonon and is defect induced (Thomsen and Reich 2000, Zólyomi et al. 2003, Kürti et al. 2002) and the G' mode is its overtone, i.e. when two phonons of the same energy are involved. The most important and unique vibration of SWCNTs is the so called Radial Breathing Mode or RBM. The motion of carbons is what the name indicates and it is depicted in the inset of Fig. 5. The principal interest in this mode comes the fact that its energy is inversely proportional to the diameter of an SWCNT (Kürti et al. 1998):

$$\nu_{\mathrm{RBM}} = C_1/d + C_2 \tag{4}$$

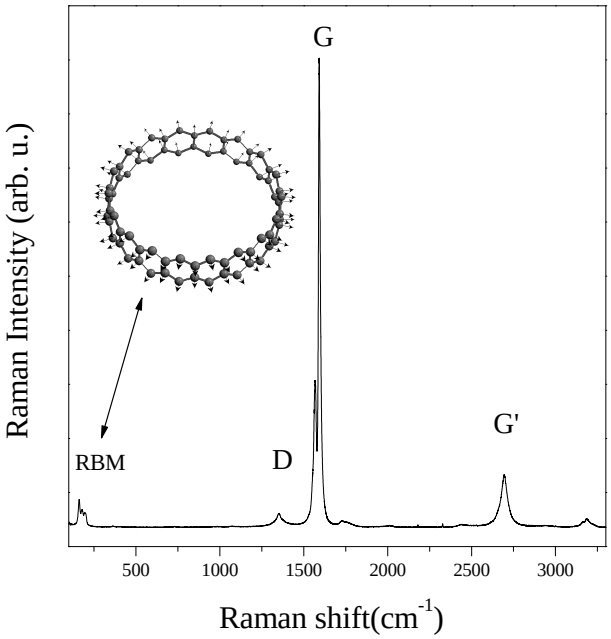

Figure 5: Raman spectrum of a typical SWCNT sample taken with $\lambda = 488$ nm (2.54 eV) laser excitation at room temperature. Labeling of the most important Raman active vibrational modes are given. Inset indicates the motion of carbons for the radial breathing mode.

where $C_1 \sim 230$ cm^{-1}nm and $C_2 \sim 10$ cm^{-1} are constants. C_2 accounts for the tube-tube interactions in the tube bundles. Eq. 4. allows to determine the diameter of the SWCNTs in a sample. E.g. for the Raman spectrum in Fig. 5., the RBM is around $\nu_{\mathrm{RBM}} \approx 170$ cm^{-1} thus it is a sample with a mean diameter of $d_{\mathrm{mean}} \approx 1.4$ nm.

2.4 Modified single-wall carbon nanotubes

As mentioned in the introduction, SWCNTs and fullerenes are both carbon allotropes with different dimensionality. A significant event which further connects nanotubes and fullerenes was the discovery of fullerene *peapods*. In 1998, Smith, Monthioux and Luzzi reported the observation of fullerenes encapsulated inside single-wall carbon nanotubes using high-resolution transmission electron microscopy (HR-TEM) (Smith et al. 1998). The schematics of the structure is shown in Fig. 6. It was suggested that fullerenes which are co-produced with the SWCNTs enter the tubes through openings and remain inside as it is energetically preferred as it was shown by first principles calculations (Melle-Franco et al. 2003, Berber et al. 2002, Otani et al. 2003, Rochefort 2003, Dubay

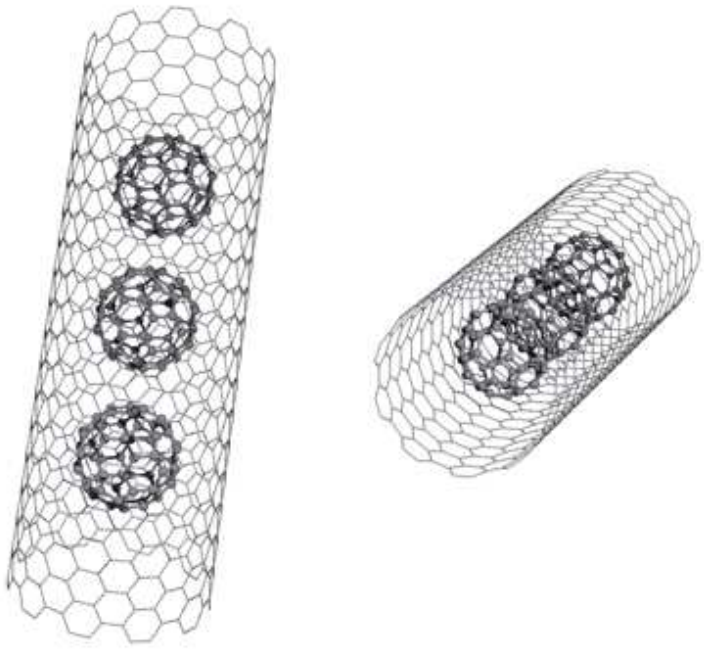

Figure 6: Schematics of the peapod structure from two viewpoints.

and Kresse 2004). The stability of this structure can be simplest understood if we consider that the nominal diameter of the C_{60}'s is 0.7 nm. Therefore an SWCNT with $d \approx 1.4$ can accommodate them so that the fullerene-tube wall distance is close to the optimal van der Waals distance of 0.335 nm (Dresselhaus et al. 1996).

It was also shown that macroscopic or close-packed filling with the fullerenes can be achieved (Smith et al. 1999, Smith and Luzzi 2000, Kataura et al. 2001). For such peapods, the presence of C_{60}s can be observed by scanning tunneling spectroscopy through the influence on the electronic properties of the tubes (Hornbaker et al. 2002). The high filling opens the way for magnetic resonance studies through encapsulation of isotope engineered fullerenes and the results are discussed herein.

The high yield synthesis of peapods is achieved by opening the SWCNTs by oxidation in air at 400-500 °C for about 0.5 hours duration. The opened SWCNTs are sealed in a glass tube together with abundant fullerene powder under vacuum. The glass tube is then heated to 650 °C for 2 hours (Kataura et al. 2001). Fullerenes sublime above $\sim$ 350 °C thus encapsulation proceeds due to the high fullerene vapor pressure inside the glass tube. Non-encapsulated fullerenes can be removed by heating the peapod material to 800 °C in dynamic

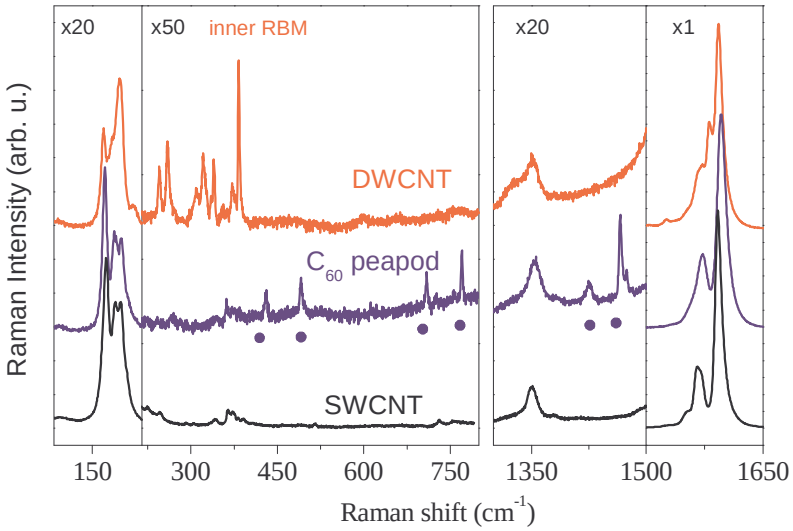

Figure 7: Transformation of peapods to DWCNTs followed by Raman spectroscopy. Note the disappearance of the fullerene modes (solid circles) and the development of narrow RBM modes in the 220-370 cm^{-1} spectral range.

vacuum or by washing in toluene. Peapods of functionalized fullerenes were also effectively encapsulated and their removal was suggested to be suitable for drug delivery (Simon et al. 2007).

The faith of fullerenes and nanotubes were further linked by the observation that upon intensive electron irradiation (Smith et al. 1999) or upon heating to 1200 °C (Smith and Luzzi 2000, Bandow et al. 2001) the encapsulated fullerenes are transformed to inner tubes. These inner tubes are single-walled carbon nanotubes such as the host outer tubes and the whole structure forms the so-called double-wall carbon nanotube (DWCNT) structure, which was extensively studied using Raman spectroscopy (Bandow et al. 2001, Pfeiffer et al. 2003, Kramberger et al. 2003). In Fig. 7., we show the changes of the Raman spectra of the tubes upon fullerene encapsulation and transformation to DWCNTs. A number of narrow lines develop in the 220-370 cm^{-1} Raman shift range which indicate the presence of smaller diameter SWCNTs with $d \approx 0.6..1$ nm according to Eq. 4. These modes were identified as the RBMs of the inner tubes (Bandow et al. 2001, Pfeiffer et al. 2003).

The inner tubes grown inside SWCNTs from peapods turned out to be a particularly interesting system as they are remarkably defect free and are isolated from the environment which results in very long phonon life-times, i.e. very narrow vibrational modes (Pfeiffer et al. 2003). In addition, their smaller diameters results in a larger spectral splitting for diameter dependent phonon modes such as e.g. the radial breathing mode. These two effects make the inner

tubes very suitable to study diameter dependent physics of the small diameter tubes with precision.

Here, we show that using ^{13}C enriched fullerenes as starting materials for the DWCNT synthesis double wall carbon nanotubes can be synthesized where the outer shell consists of natural carbon whereas the inner shell is ^{13}C enriched. This allows a nanotube specific enrichment. Usual ^{13}C enrichment of nanotubes involves their synthesis from enriched graphite (Tang et al. 2000, Rümmeli et al. 2007). However, the resulting material contains other carbonaceous phases, such as graphite nanoparticles which are also isotope enriched. The use of the isotope engineered DWCNTs is two-fold: on one hand they facilitate identification of inner tube Raman modes on the other hand they are excellent probes for nuclear magnetic resonance which requires the presence of a sizeable amount of ^{13}C isotope.

Alternatively, DWCNTs can be produced with usual synthesis methods such as arc-discharge (Hutchison et al. 2001) or Chemical Vapor Deposition, CVD, (Ren et al. 2002) under special conditions. However, such methods do not allow SWCNT specific isotope enrichment and the side-product carbon phases are also isotope enriched. Therefore such methods are not considered as isotope engineering.

3 Isotope engineering of single-wall carbon nanotubes

3.1 SWCNT specific isotope engineering

The ability to grow inner tubes from encapsulated fullerenes provided the idea to grow inner tubes from isotope enriched fullerenes. Such fullerenes are available commercially (MER Corp., Tucson, USA) and are produced by the standard Krätschmer-Huffmann process (Krätschmer et al. 1990), i.e. by an arc-discharge synthesis from ^{13}C graphite rods. Two supplier specified grades of ^{13}C enriched fullerene mixtures were used: 25 and 89 %. These are mean values of the enrichment and the number of ^{13}C nuclei for a given fullerene follows a binomial (or with a good approximation a Poisson) distribution. These enrichment values were refined using Raman spectroscopy. The above detailed standard routes were followed for the peapod and DWCNT synthesis: SWCNTs were opened by oxidation in air, were placed inside glass tubes with excess fullerenes and were finally subject to a 1250 °C heat treatment for 1 hour for the DWCNT transformation (Simon et al. 2005). As we discuss here, this results in a compelling isotope engineered system: double-wall carbon nanotubes with ^{13}C isotope enriched inner walls and outer walls containing natural carbon (Simon et al. 2005).

In Fig. 8, we show the inner tube RBM range Raman spectra for a natural DWCNT and two DWCNTs with differently enriched inner walls, 25 % and 89 %. These two latter samples are denoted as $^{13}C_{25}$- and $^{13}C_{89}$-DWCNT, respectively. The inner wall enrichment is taken from the nominal enrichment of the fullerenes used for the peapod production, whose value is slightly refined

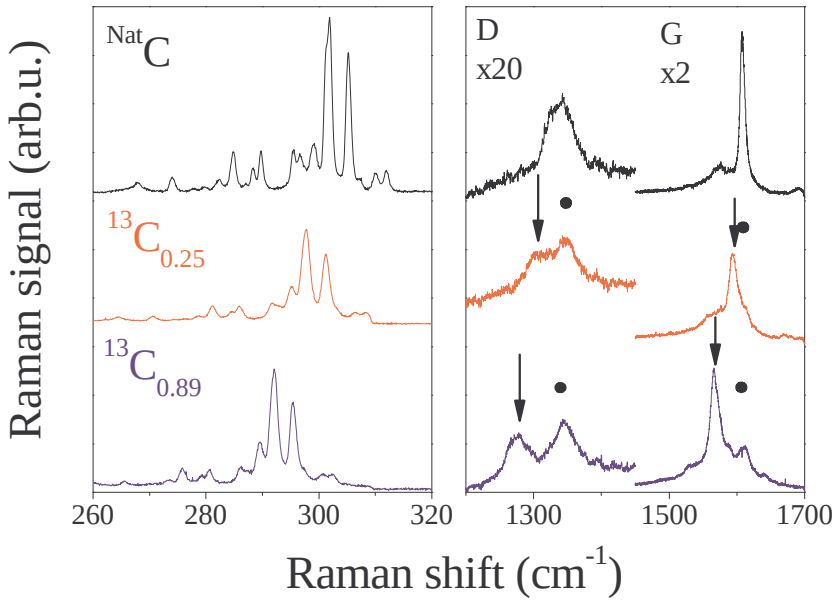

Figure 8: Raman spectra of DWCNTs with natural carbon and ^{13}C enriched inner tubes at 676 nm laser excitation and 90 K. The inner tube RBM and D and G mode spectral ranges are shown. Arrows and filled circles indicate the D and G modes corresponding to the inner and outer tubes, respectively. Reprinted figure with permission from F. Simon *et al.* Phys. Rev. Lett. **95**, 017401 (2005). Copyright (2005) by the American Physical Society.

based on the Raman data. An overall downshift of the inner tube RBMs is observed for the ^{13}C enriched materials accompanied by a broadening of the lines. The downshift is clear evidence for the effective ^{13}C enrichment of inner tubes. The magnitude of the enrichment and the origin of the broadening are discussed below.

The RBM lines are well separated for inner and outer tubes due to the $\nu_{\rm RBM} \propto 1/d$ relation and a mean inner tube diameter of $d \sim 0.7$ nm (Abe et al. 2003, Simon et al. 2005). However, other vibrational modes such as the defect induced D and the tangential G modes strongly overlap for inner and outer tubes. Arrows in Fig. 8. indicate a gradually downshifting component of the observed D and G modes. These components are assigned to the D and G modes of the inner tubes. The sharper appearance of the inner tube G mode, as compared to the response from the outer tubes, is related to the excitation of semiconducting inner tubes and metallic outer tubes (Pfeiffer et al. 2003, Simon et al. 2005).

The shifts for the RBM, D and G modes can be analyzed for the two grades of

enrichment. The average value of the relative shift for these modes was found to be $(\nu_0 - \nu)/\nu_0 = 0.0109(3)$ and $0.0322(3)$ for the $^{13}C_{0.25}$- and $^{13}C_{0.89}$-DWCNT samples, respectively. Here, ν_0 and ν are the Raman shifts of the same inner tube mode in the natural carbon and enriched materials, respectively. In the simplest continuum model, the shift originates from the increased mass of the inner tube walls. This gives:

$$(\nu_0 - \nu)/\nu_0 = 1 - \sqrt{\frac{12 + c_0}{12 + c}}, \tag{5}$$

where c is the concentration of the ^{13}C enrichment on the inner tube, and $c_0 = 0.011$ is the natural abundance of ^{13}C in carbon. The resulting values of c are 0.277(7) and 0.824(8) for the 25 and 89 % samples, respectively.

The growth of isotope labeled inner tubes allows to address whether carbon exchange between the two walls occurs during the inner tube growth. In Fig. 9, we show the G' spectral range for DWCNTs with natural carbon and ^{13}C enriched inner walls with 515 nm laser excitation. The G' mode of DWCNTs corresponds to the two-phonon process of the defect induced D mode. The upper G' mode component corresponds to the outer tubes and the lower to the inner tubes. The outer tube G' components are unaffected by the ^{13}C enrichment within the 1 cm^{-1} experimental accuracy. This gives an upper limit to the extra ^{13}C in the outer wall of 1.4 %. This proves that there is no sizeable carbon exchange between the two walls as this would result in a measurable ^{13}C content on the outer wall, too. We show the schematics of the isotope engineered DWCNTs in Fig. 10.

This result important for the contrast of the NMR signal between the two walls as it is discussed further below: were the outer shell also enriched, one could not obtain a reliable information about the density of states on the inner shell alone.

The narrow RBMs of inner tubes and the freedom to control their isotope enrichment allows to precisely compare the isotope related phonon energy changes in the experiment and in *ab-initio* calculations. This was performed by J. Kürti and V. Zólyomi (Simon et al. 2005). The validity of the above simple continuum model in Eq. 5. for the RBM frequencies was verified by performing first principles calculations on the (5,5) tube as an example. In the calculation, the Hessian matrix was determined by DFT using the Vienna Ab Initio Simulation Package (Kresse and Joubert 1999). Then, a large number of random ^{13}C distributions were generated and the RBM vibrational frequencies were determined from the diagonalization of the corresponding dynamical matrix for each individual distribution. The distribution of the resulting RBM frequencies can be approximated by a Gaussian where center and variance determine the isotope shifted RBM frequency and the spread in these frequencies. The difference between the shift determined from the continuum model and from the *ab-initio* calculations is below 1 %.

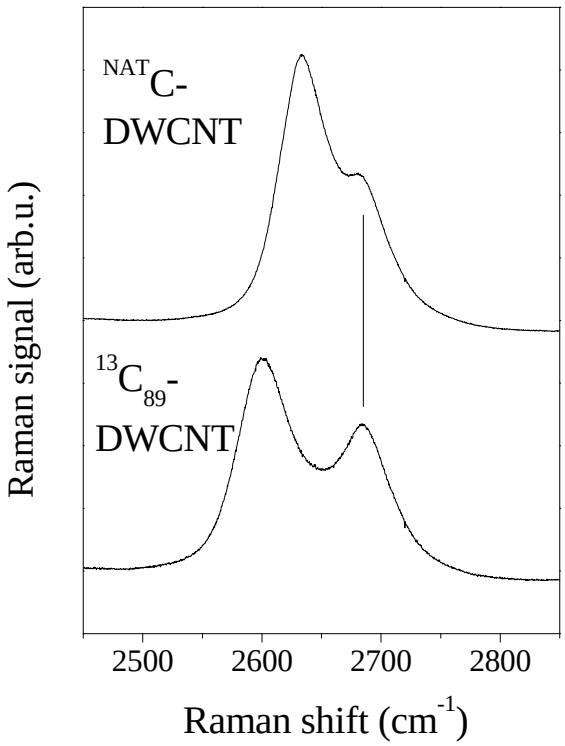

Figure 9: G' spectral range of DWCNTs with natural carbon and ^{13}C enriched inner walls with 515 nm laser excitation. Note the unchanged position of the outer tube G' mode indicated by a vertical line.

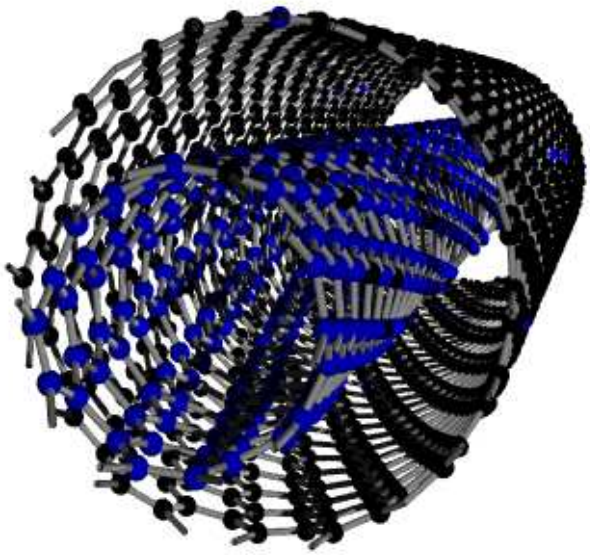

Figure 10: Schematic structure of an isotope engineered DWCNT with (14,6) outer and (6,4) inner tubes. ^{12}C and ^{13}C are shown in black and blue, respectively. The inner tube is 89 % ^{13}C enriched and the outer contains natural carbon (1.1 % ^{13}C abundance), which are randomly distributed for both shells.

3.2 Growth mechanism of inner tubes

The growth of inner tubes from fullerenes raises the question, whether the fullerene geometry plays an important role in the inner tube growth or it acts as a carbon source only. According to the first scenario, inner tube growth starts with the bond formation between adjacent fullerenes and the low energy "bond-jumping" Stone-Wales transformation (Stone and Wales 1986) proceeds the reaction until a tube-like structure is attained. The second scenario suggests that fullerene geometry plays no particular role and it acts as a carbon source only, fullerenes fully disintegrate into small units such as gaseous C_2 inside the host outer tubes and fuse together to form the inner tubes. Theoretical results favor the first possibility (Zhao et al. 2002, Han et al. 2004) as it was found that the Stone-Wales transformations requires little energy.

An earlier experimental work found that inner tube growth starts with the formation of inner tubes with $d \approx 0.7$ nm which change their diameter for longer heat treatments (Bandow et al. 2004). This finding also favors the first

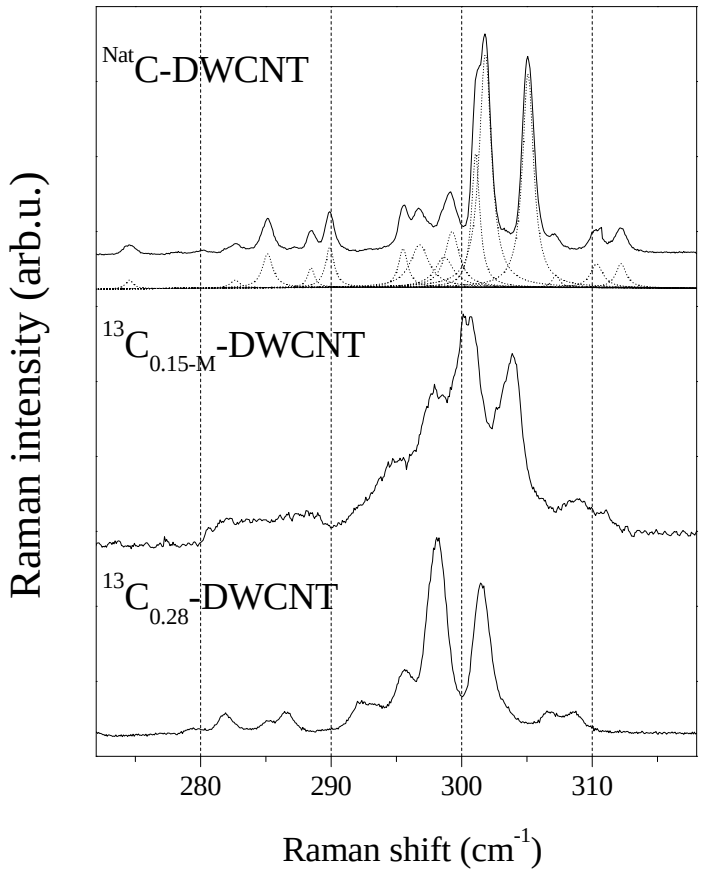

Figure 11: Raman spectra of DWCNTs with $^{\rm Nat}$C, $^{13}C_{28}$ and $^{13}C_{15-M}$ enriched inner tubes at λ=676 nm laser excitation and 90 K measured with high resolution. We show deconvolution of the DWCNT inner tube RBMs into components for the natural carbon sample. Vertical dashed lines are intended to guide the eye. Reprinted figure with permission from V. Zólyomi *et al.* Phys. Rev. B **75**, 195419 (2007). Copyright (2007) by the American Physical Society.

possibility as the diameter of C_{60} is 0.7 nm which is not optimal when the host outer tube has $d = 1.4$ nm concerning that the tube-shell to tube-shell distance is the Van der Waals separation of 0.335 nm. The growth of the inner tubes from the isotope enriched fullerenes allows to distinguish between the two scenarios as we present it here.

The presence of ^{13}C isotopes on the inner tubes shifts the energy of the vibrational modes as we discussed it above. However, in addition to the shift, inhomogeneous broadening of the vibrational modes also occurs as the ^{13}C iso-

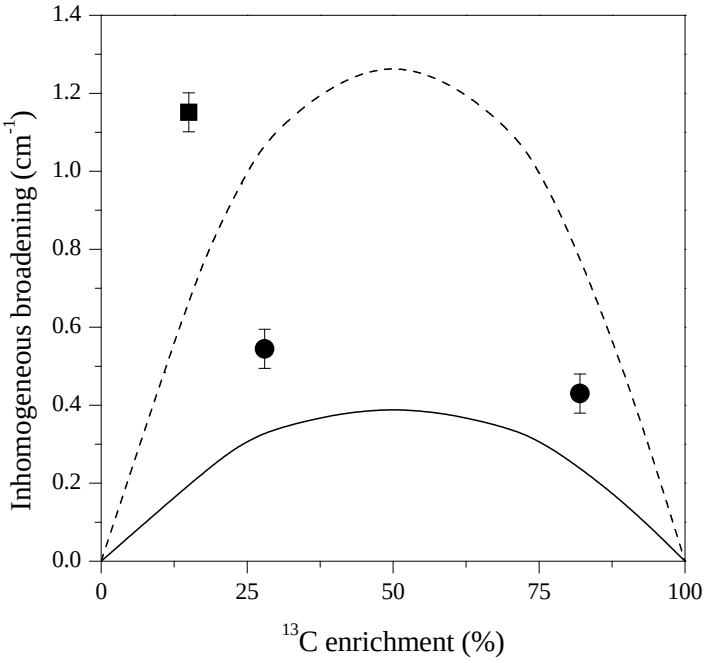

Figure 12: Measured (symbols) and calculated (solid and dashed curves) inhomogeneous broadening of isotope engineered inner tubes as a function of the ^{13}C enrichment. ■: $^{13}C_{0.28}$- and $^{13}C_{0.82}$-DWCNT, •: $^{13}C_{0.15-M}$-DWCNT. Solid and dashed curves are calculated inhomogeneous broadening for a (5,5) inner tube for the uniform and mixed distributions, respectively. Reprinted figure with permission from V. Zólyomi *et al.* Phys. Rev. B **75**, 195419 (2007). Copyright (2007) by the American Physical Society.

tope distribution is statistically random along the tube axis. This effect is best observed on the inner tube RBM lines which are very narrow, their HWHM can be as small as 0.5 cm^{-1}. Regions which are somewhat richer in ^{13}C give more downshifted modes than those poorer in ^{13}C. To study the effect of isotope inhomogeneity, we consider two types of experiments. In the first one, we encapsulate ^{13}C fullerenes inside the host outer tubes and grow the inner tubes. We call this system $^{13}C_{0.28}$-DWCNT and we refer to this material as having a uniform isotope distribution. In the second experiment, we prepare a 1:1 mixture of $^{13}C_{0.28}$-C_{60} with C_{60} of natural carbon. We call this second systems as having a mixed isotope distribution. Clearly, for the second experiment the enriched and natural fullerenes enter the host outer tubes in a random fashion and we call the resulting DWCNTs as $^{13}C_{0.15-M}$-DWCNT. The resulting RBM modes for the two kinds of experiments is shown in Fig. 11. along with the data on the inner tubes based on natural C_{60}.

We observe that the inner tube RBMs are narrowest for the natural carbon sample, they are significantly broadened for the $^{13}C_{0.15-M}$-DWCNT sample, and somewhat less broadened for the $^{13}C_{0.28}$-DWCNT material. The resulting inhomogeneous broadenings are summarized in Fig. 12. V. Zólyomi et al. attempted to reproduce the observed data with first principles calculations (Zólyomi et al. 2007). A (5,5) inner tube was considered which has a 20 atom unit cell. For the uniform isotope enrichment, it was assumed that a 60 atom, i.e. 3 unit cells contain an amount of ^{13}C isotopes which correspond to the nominal enrichment, r, but the exact amount of the isotopes follows the binomial distribution: $p(n_{13} = k) = \binom{60}{k} r^k (1-r)^{60-k}$, where $p(n_{13} = k)$ is the probability of finding k ^{13}C's isotopes in the 3 unit cells.

A large number of such configurations were generated and the resulting RBM frequencies were calculated whose distribution gave the inhomogeneous broadening. The result is shown as a solid curve in Fig. 12. For the mixed distribution, it was assumed that 3 unit cell entities are randomly distributed where some 3 unit cell entity contains is enriched and other 3 unit cell entities are of natural carbon. The distribution of these 3 unit cell entities was also considered as random which reflects the real situation that natural and enriched fullerenes are located in a random fashion along the outer host tube axis. The result of this calculation is shown with a dashed curve in Fig. 12.

Some general properties can be drawn from the result. First, both kinds of broadenings are symmetric for the 50 % enrichment and are monotonously increasing for the 1-50 % enrichment. Second, the mixed distribution calculation gives about a factor 3 larger inhomogeneous broadening than the uniform one. For both kinds of calculations the resulting inhomogeneous broadening is about a factor two smaller than the experimental broadening. However, if both calculated curves are multiplied by the same amount (by 1.65) a close agreement between the calculation and the experiment is found (not shown). This means that the above models of uniform and mixed distribution properly account for the experimentally observed inhomogeneous broadening.

This agreement has an important consequence for the inner tube growth. The mixed model assumed that carbon from the fullerenes are fixed to the locations of their fullerene "mother"-compound. If carbons were diffusing during the inner tube growth, one would expect a significantly smaller inhomogeneous broadening for the mixed sample which is clearly not the case. The broadening for the $^{13}C_{15-M}$-DWCNT sample is about 3.5 times larger than for a uniformly enriched $^{13}C_{15}$-DWCNT material. This means that the data and its theoretical explanation rules out any carbon diffusion during the inner tube growth. In turn, this supports the above model of inner tube growth due to fullerene fusion and Stone-Wales transformations rather than due to a complete disintegration into small carbon units.

3.3 NMR studies on isotope engineered heteronuclear nanotubes

The growth of the "isotope engineered" nanotubes, i.e. DWCNTs with highly enriched inner wall allows to study these samples with NMR with an unprecedented specificity for the small diameter carbon nanotubes. For normal SWCNTs, either grown from natural or ^{13}C enriched carbon, the NMR signal originates from all kinds of carbon like amorphous or graphitic carbon.

NMR is usually an excellent technique for probing the electronic properties at the Fermi level of metallic systems. The examples include conducting polymers, fullerenes, and high temperature superconductors. However the 1.1% natural abundance of ^{13}C with nuclear spin I=1/2 limits the sensitivity of such experiments. As a result, meaningful NMR experiments has to be performed on ^{13}C isotope enriched samples. NMR data were taken with the samples sealed in quartz tubes filled with a low pressure of high purity Helium gas (Simon et al. 2005).

NMR allows to determine the amount of enriched tubes in our sample as it is sensitive to the number of ^{13}C nuclei. In Fig. 13, we show the static and magic angle spinning, MAS, spectra of ^{13}C enriched DWCNTs, and the static spectrum for the SWCNT material. The mass fraction which belongs to the highly enriched phase can be calculated from the integrated signal intensity by comparing it to the signal intensity of the 89 % ^{13}C enriched fullerene material. We found that the mass fraction of the highly enriched phase relative to the total sample mass is 13(4) %. The expected mass ratio of inner tubes as compared to the total sample mass is 15 %, which is obtained from the SWCNT purity (50 %), the ∼70 % volume filling for peapod samples (Liu et al. 2002), and the mass ratio of encapsulated fullerenes to the mass of the SWCNTs. Thus, the measured mass fraction of the highly enriched phase is very similar to that of the calculated mass fraction of inner tubes. This proves that the NMR signal comes nominally from the inner tubes.

The typical chemical shift anisotropy (CSA) powder pattern is observed for the SWCNT sample in agreement with previous reports (Tang et al. 2000, Goze-Bac et al. 2002). However, the static DWCNT spectrum cannot be explained with a simple CSA powder pattern even if the spectrum is dominated by the inner tube signal. The complicated spectral structure suggests that the chemical shift tensor parameters are distributed for the inner tubes. It is the result of the higher curvature of inner tubes as compared to the outer ones: the variance of the diameter distribution is the same for the inner and outer tubes (Simon et al. 2005) but the corresponding bonding angles show a larger variation (Kürti et al. 2003). In addition, the residual line-width in the MAS experiment, which is a measure of the sample inhomogeneity, is 60(3) ppm, i.e. about twice as large as the ∼35 ppm found previously for SWCNT samples (Tang et al. 2000, Goze-Bac et al. 2002). The isotropic line position, determined from the MAS measurement, is 111(2) ppm. This value is significantly smaller than the isotropic shift of the SWCNT samples of 125 ppm (Tang et al. 2000, Goze-Bac et al. 2002). However, recent theoretical *ab-initio* calculations successfully

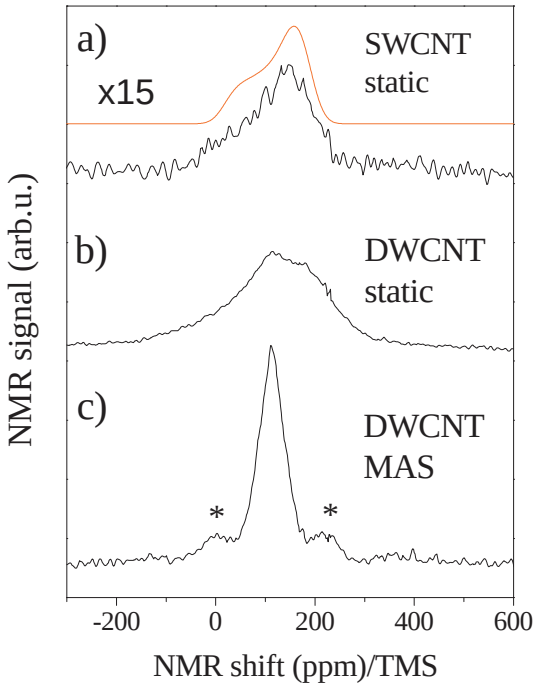

Figure 13: NMR spectra normalized by the total sample mass, taken with respect to the tetramethylsilane (TMS) shift. (a) Static spectrum for non-enriched SWCNT enlarged by 15. Smooth solid line is a chemical shift anisotropy powder pattern simulation with parameters published in the literature (Tang et al. 2000). (b) Static and (c) MAS spectra of $^{13}C_{0.89}$-DWCNT, respectively. Asterisks show the sidebands at the 8 kHz spinning frequency. Reprinted figure with permission from F. Simon *et al.* Phys. Rev. Lett. **95**, 017401 (2005). Copyright (2005) by the American Physical Society.

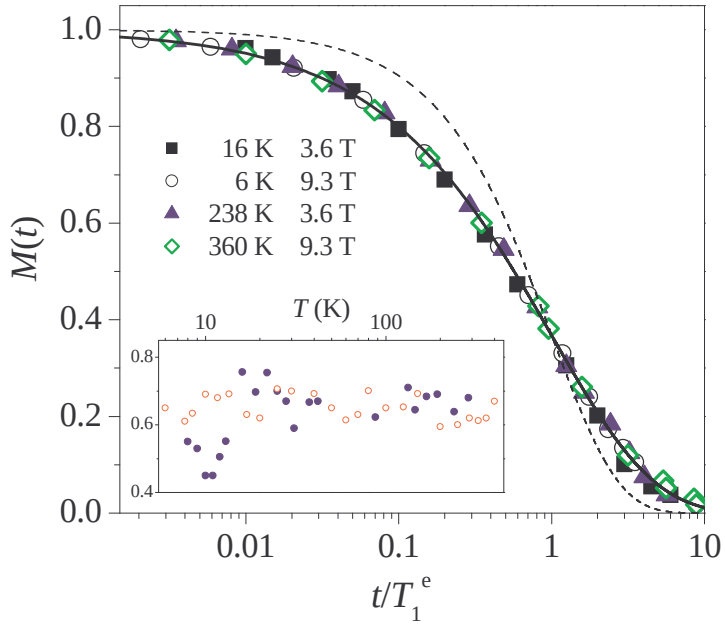

Figure 14: Reduced nuclear magnetization recovery, $M(t)$, as a function of the scaled delay time t/T_1^e for various temperature and magnetic field values. Both axes are dimensionless. Solid curve shows stretched exponential fit with $\beta = 0.65$ and dashed curve shows single exponential with $\beta = 1$. Inset shows temperature dependence of the best fit values of β at 3.6 Tesla ($\bullet$) and 9.3 Tesla ($\circ$), and average value of the data set $\beta = 0.65$ (solid line). Reprinted figure with permission from P. M. Singer *et al.* Phys. Rev. Lett. **95**, 236403 (2005). Copyright (2005) by the American Physical Society.

explained this anomalous isotropic chemical shift (Marques et al. 2006). It was found that diamagnetic demagnetizing currents on the outer walls cause the diamagnetic shift of the inner tube NMR signal.

The dynamics of the nuclear relaxation is a sensitive probe of the local electronic properties (Slichter 1989). As NMR is a low energy ($\hbar\omega \approx 0.3\mu$eV for ^{13}C in 7 T field) method, it is only sensitive to the immediate vicinity of the Fermi surface. It can be probed using the spin lattice relaxation time, T_1, defined as the characteristic time it takes the ^{13}C nuclear magnetization to recover after saturation (Singer et al. 2005). The signal intensity after saturation, $S(t)$, is deduced by integrating the fast Fourier transform of half the spin-echo for different delay times t. The value of T_1 can be obtained by fitting the t dependence of $S(t)$ to the form $S(t) = S_a - S_b \cdot M(t)$, where $S_a \simeq S_b$ (> 0) are arbitrary

signal amplitudes, and

$$M(t) = \exp\left[-\left(t/T_1^e\right)^{\beta}\right], \tag{6}$$

is the reduced magnetization recovery of the ^{13}C nuclear spins. Fig. 14 shows the results of $M(t)$ for the inner-tubes as a function of the scaled delay time t/T_1^e, under various experimental conditions listed in the Figure. $M(t)$ does not follow the single exponential form with $\beta = 1$ (dashed line), but instead fits well to a stretched exponential form with $\beta \simeq 0.65(5)$, implying a distribution in the relaxation times T_1.

The data in Fig. 14 is displayed on a semi-log scale for the time axis in order to emphasize the data for earlier decay times and to illustrate the collapse of the data set for the upper 90 % of the NMR signal. For a broad range of experimental conditions, the upper 90 % of the $M(t)$ data is consistent with constant $\beta \simeq 0.65(5)$ (see inset), implying a field and temperature independent underlying distribution in T_1. The lower 10 % of the $M(t)$ data, corresponding to longer delay times, comes from the non-enriched outer-walls which have much longer relaxation times under similar experimental conditions (Tang et al. 2000, Goze-Bac et al. 2002).

The collapse of the data set in Fig. 14 to Eq. (6) with constant $\beta = 0.65(5)$ is a remarkable experimental observation. From an experimental point of view, it implies that all one needs in order to characterize the T and H dependence of the underlying T_1 distribution is the bulk (or average) value, T_1^e (Eq. (6)). From an interpretational point of view, it implies that each inner-tube in the powder sample has a different value of T_1, yet *all* the T_1 components and therefore all the inner-tubes follow the same T and H dependence within experimental uncertainty. This finding is in contrast to earlier reports in SWCNTs where $M(t)$ fits well to a bi-exponential distribution, 1/3 of which had a short T_1 value characteristic of fast relaxation from metallic tubes, and the remaining 2/3 had long T_1 corresponding to the semiconducting tubes (Tang et al. 2000, Goze-Bac et al. 2002, Shimoda et al. 2002, Kleinhammes et al. 2003), as expected from a macroscopic sample of SWCNTs with random chiralities. The data for the inner-tubes in DWCNTs differ in that a similar bi-exponential fit to $M(t)$ is inconsistent with the shape of the recovery in Fig. 14. Furthermore, if there were 1/3 metallic and 2/3 truly semi-conducting inner-tubes in the DWCNT sample, one would expect the ratio of T_1 between semiconducting and metallic tubes to increase exponentially with decreasing T below the semiconducting gap ($\sim$ 5000 K). As a consequence, one expects an increasingly large change in the underlying distribution in T_1 with decreasing T. This change would manifest itself as a large change in the shape of the $M(t)$, however this is not the case as shown in Fig. 14. The possibility of two components in T_1 with different T dependence can therefore be ruled out, and instead it could be concluded that all T_1 components (corresponding to distinct inner-tubes) exhibit the same T and H dependence within experimental scattering.

The experimentally observed uniform metallicity of inner tubes is a surpris-

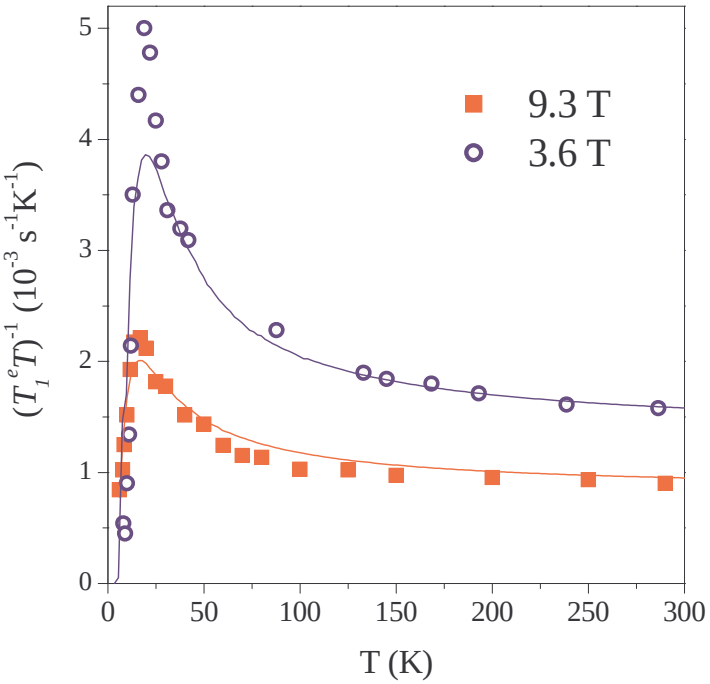

Figure 15: Temperature dependence of spin-lattice relaxation rate divided by temperature, $1/T_1^e T$, in units of $(10^3 \times$ s^{-1} K $^{-1})$. Grey curves are best fits to Eq. (8) with $2\Delta = 46.8(40.2)$ K for $H = 3.6(9.3)$ Tesla, respectively. Reprinted figure with permission from P. M. Singer *et al.* Phys. Rev. Lett. **95**, 236403 (2005). Copyright (2005) by the American Physical Society.

ing observation. This is suggested to be caused by the shifting of the inner tube Fermi levels due to charge transfer between the two tube walls. Indeed, *ab-initio* calculations found that charge transfer and hybridization can render an otherwise semiconducting tube metallic (Okada and Oshiyama 2003, Zólyomi et al. 2008).

With these arguments, the bulk average T_1^e defined in Eq. (6) is considered and its uniform T and H dependence can be followed. The $M(t)$ data can be fitted with the constant exponent $\beta = 0.65(5)$, which reduces unnecessary experimental scattering in T_1^e. In Fig. 15 we show the temperature dependence of $1/T_1^e T$ in for two different values of the external magnetic field H. The data can be separated into two temperature regimes; the high temperature regime $\gtrsim$ 150 K, and the low T regime $\lesssim$ 150 K. At high temperatures, $1/T_1^e T$ is independent of T which indicates a metallic state (Slichter 1989) for all of the inner tubes.

The simplest explanation for the experimental data in a non-interacting

electron model of a 1D semiconductor with a small secondary gap (SG). The SG may be a result of the finite inner-wall curvature (Hamada et al. 1992, Kane and Mele 1997, Mintmire and White 1998, Zólyomi and Kürti 2004). The $1/T_1^eT$ data can be fitted using this non-interacting model with only one free parameter, the homogeneous SG, 2Δ. The normalized form of the gapped 1D density-of-states $n(E)$

$$n(E) \;=\; \begin{cases} \frac{E}{\sqrt{E^2-\Delta^2}} & \text{for } |E|>\Delta \\ 0 & \text{otherwise} \end{cases} \tag{7}$$

here, E is taken with respect to the Fermi energy). Eq. (7) is used to calculate $1/T_1^eT$ (Moriya 1963) as such

$$\frac{1}{T_1^eT} \;=\; \alpha(\omega)\int_{-\infty}^{\infty} n(E)n(E+\omega)\left(-\frac{\delta f}{\delta E}\right)dE, \tag{8}$$

where E and ω are in temperature units for clarity, f is the Fermi function $f=[\exp(E/T)+1]^{-1}$, and the amplitude factor $\alpha(\omega)$ is the high temperature value for $1/T_1^eT$. The results of the best fit of the data to Eq. (8) are presented in Fig. 15, where $2\Delta = 43(3)$ K ($\equiv 3.7$ meV) is H independent within experimental scattering between 9.3 and 3.6 Tesla.

The explanation in the non-interacting electron picture have two shortcomings: i) calculations show that SG is of the order of a few 100 meV, which is two orders of magnitude larger than the experimental value, ii) the SG is expected to be strongly chirality dependent. In fact, a gap induced by electron-electron or electron-phonon correlations could be of the right order of magnitude (Bohnen et al. 2004, Connétable et al. 2005) and it could be uniform, i.e. chirality independent. The problem with such a correlation induced gap is its magnitude: experimentally, the gap is open above 300 K, thus the critical transition of the correlation is $T_c > 300$ K. However, a mean-field expression between the gap and the critical temperature usually satisfies that: $2\Delta/T_c > 3.52$ (Bardeen et al. 1957) but the current value is 0.13 or smaller. To avoid this contradiction, the NMR data was reinterpreted in the framework of the Tomonaga-Luttinger liquid theory (Dóra et al. 2007), which we outline here.

The TLL state occurs in one-dimensional systems with strong electron-electron correlation. Formally, the interacting electrons can be treated with a non-interacting bosonic Hamiltonian which contain two TLL parameters $K_c \approx 0.2$ for the charge and $K_s \approx 1$ for the spin degree of freedom. The physically relevant correlation functions, such as e.g. the spin-spin or current-current correlation functions follow power law dependencies with exponents related to the TLL parameters. This leads to power law behavior in the experimental measurables as e.g. $(T_1T)^{-1} \propto T^{-1}$. The latter result can be qualitatively explained by the localization of electrons in the TLL state, which leads to a paramagnetic-like fluctuating fields, giving the increase of $(T_1T)^{-1}$ with decreasing temperature (Abragam 1961). The apparent presence of the gap at low temperatures was explained by the formation of the so-called Luther-Emery liquid (Dóra et al. 2007), which is a ground state which contains a gap in the excitation spectrum and

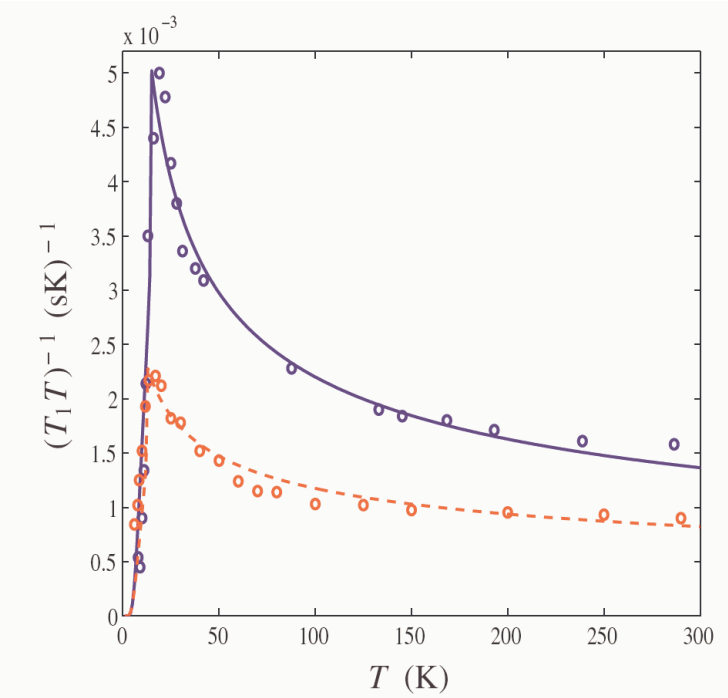

Figure 16: Calculated $(T_1T)^{-1}$ assuming a TLL ground state of the electrons in the inner tube SWCNTs. The magnetic field dependence is associated to the slight field dependence of the K_s TLL parameter. Reprinted figure with permission from Dóra *et al.* Phys. Rev. Lett. **99**, 166402 (2007). Copyright (2007) by the American Physical Society.

competes with the TLL state.

We show the calculated $(T_1T)^{-1}$ values in Fig. 16. Although, the calculation relies on essentially three parameters only (the two TLL and a vertical scaling parameter, the gap being fixed to the temperature where the gap opens) we observe a much better agreement between the data and the calculation as compared to the gapped Fermi-liquid explanation shown in Fig. 15. This shows that the TLL description is indeed relevant in describing the NMR data.

Summarizing the NMR studies on DWCNTs, it was shown that T_1 has a similar T and H dependence for all the inner-tubes with no indication of a metallic/semiconducting separation due to chirality distributions. Below ∼150 K, $1/T_1^eT$ increases dramatically with decreasing T and a gap in the spin excitation spectrum is found below $\Delta \simeq 20$ K. The result can be understood if electrons on the inner tubes are in the Tomonaga-Luttinger liquid state above 20 K and in the Luther-Emery liquid state below. This makes SWCNTs the only known example of materials where the TLL state is observed using NMR.

4 Summary

In summary, we reviewed recent advances in the isotope engineering of single-wall carbon nanotubes. We showed how nanotube specific ^{13}C isotope enrichment can be achieved by encapsulating ^{13}C enriched fullerenes inside host SWCNTs and by transforming them into a smaller inner nanotube. The process produces highly ^{13}C enriched inner tubes while the host outer tube and other carbonaceous side-products in the SWCNT sample consists of natural carbon. This material allows to identify Raman modes of the double-wall carbon nanotubes. The use of mixtures of natural and ^{13}C enriched fullerenes allows to prove that no diffusion of carbon happens along the nanotube axis during inner nanotube synthesis, which supports the fullerene fusion model for their growth. The isotope enriched inner tubes are excellent for nuclear magnetic resonance studies. Measurement of the ^{13}C NMR T_1 relaxation time allows to identify a non Fermi liquid behavior above 20 K and a low energy, correlation related gap providing direct experimental evidence for the Tomonaga-Luttinger liquid state in single-wall carbon nanotubes.

5 Acknowledgements

This work was supported by the Hungarian State Grants No. F61733 and NK60984, and by the Bolyai postdoctoral fellowship of the Hungarian Academy of Sciences. H. Kuzmany, R. Pfeiffer, T. Pichler, M. Rümmeli, C. Kramberger, H. Alloul, P. M. Singer, P. Wzietek, B. Dóra, M. Gulácsi, J. Bernardi, F. Fülöp, A. Rockenbauer, A. Jánossy, L. Forró, V. N. Popov, J. Koltai, V. Zólyomi and J. Kürti are acknowledged for their participation in the reviewed works. Dario Quintavalle is acknowledged for preparing some of the figures.

References

Abe, M., Kataura, H., Kira, H., Kodama, T., Suzuki, S., Achiba, Y., Kato, K.-i., Takata, M., Fujiwara, A., Matsuda, K. and Maniwa, Y. (2003). Structural transformation from single-wall to double-wall carbon nanotube bundles, *Phys. Rev. B* **68**: 041405(R).

Abragam, A. (1961). *Principles of Nuclear Magnetism*, Oxford University Press, Oxford, England.

Arnold, M., Green, A., Hulvat, J., Stupp, S. and Hersam, M. (2006). Sorting Carbon Nanotubes by Electronic Structure via Density Differentiation, *Nature Nanotech.* **1**: 60–65.

Bachilo, S. M., Strano, M. S., Kittrell, C., Hauge, R. H., Smalley, R. E. and Weisman, R. B. (2002). Structure-Assigned Optical Spectra of Single-Walled Carbon Nanotubes, *Science* **298**: 2361–2366.

Bachtold, A., Hadley, P., Nakanishi, T. and Dekker, C. (2001). Logic circuits with carbon nanotube transistors, *Science* **294**: 1317–1320.

Bandow, S., Hiraoka, T., Yumura, T., Hirahara, K., Shinohara, H. and Iijima, S. (2004). Raman scattering study on fullerene derived intermediates formed within single-wall carbon nanotube, *Chem. Phys. Lett.* **384**: 320.

Bandow, S., Takizawa, M., Hirahara, K., Yudasaka, M. and Iijima, S. (2001). Raman scattering study of double-wall carbon nanotubes derived from the chains of fullerenes in single-wall carbon nanotubes, *Chem. Phys. Lett.* **337**: 48–54.

Bardeen, J., Cooper, L. N. and Schrieffer, J. R. (1957). Theory of Superconductivity, *Phys. Rev.* **108**: 1175–1204.

Berber, S., Kwon, Y.-K. and Tománek, D. (2002). Microscopic Formation Mechanism of Nanotube Peapods, *Phys. Rev. Lett.* **88**: 185502.

Bethune, D. S., Kiang, C. H., DeVries, M. S., Gorman, G., Savoy, R. and Beyers, R. (1993). Cobalt-catalysed growth of carbon nanotubes with single-atomic-layer walls, *Nature* **363**: 605.

Bockrath, M., Cobden, D. H., Lu, J., G., R. A., Smalley, R. E., Balents, L. and McEuen, P. L. (1999). Luttinger-liquid behaviour in carbon nanotubes, *Nature* **397**: 598 – 601.

Bohnen, K. P., Heid, R., Liu, H. J. and Chan, C. T. (2004). Lattice Dynamics and Electron-Phonon Interaction in (3,3) Carbon Nanotubes, *Phys. Rev. Lett.* **93**: 245501–1–4.

Capinski, W. S., Maris, H. J., Bauser, E., Silier, I., Asen-Palmer, M., Ruf, T., Cardona, M. and Gmelin, E. (1997). Thermal conductivity of isotopically enriched Si, *Appl. Phys. Lett.* **71**: 2109–2111.

Chattopadhyay, D., Galeska, L. and Papadimitrakopoulos, F. (2003). A route for bulk separation of semiconducting from metallic single-wall carbon nanotubes, *J. Am. Chem. Soc.* **125**: 3370–3375.

Chen, Z. H., Du, X., Du, M. H., Rancken, C. D., Cheng, H. P. and Rinzler, A. G. (2003). , *Nano Lett.* **3**: 1245–1259.

Connétable, D., Rignanese, G.-M., Charlier, J.-C. and Blase, X. (2005). Room Temperature Peierls Distortion in Small Diameter Nanotubes, *Phys. Rev. Lett.* **94**: 015503–1–4.

Dóra, B., Gulácsi, M., Simon, F. and Kuzmany, H. (2007). Spin gap and Luttinger liquid description of the NMR relaxation in carbon nanotubes, *Phys. Rev. Lett.* **99**: 166402–1–4.

Dresselhaus, M., Dresselhaus, G. and Ecklund, P. C. (1996). *Science of Fullerenes and Carbon Nanotubes*, Academic Press.

Dresselhaus, M. S., Dresselhaus, G. and Avouris, P. (2001). *Carbon Nanotubes: Synthesis, Structure, Properties, and Applications*, Springer, Berlin, Heidelberg, New York.

Dubay, O. and Kresse, G. (2004). Density functional calculations for C_{60} peapods, *Phys. Rev. B* **70**: 165424.

Egger, R. and Gogolin, A. O. (1997). Effective low-energy theory for correlated carbon nanotubes, *Nature* **79**: 50825085.

Fantini, C., Jorio, A., Souza, M., Strano, M. S., Dresselhaus, M. S. and Pimenta, M. A. (2004). Optical Transition Energies for Carbon Nanotubes from Resonant Raman Spectroscopy: Environment and Temperature Effects, *Phys. Rev. Lett.* **93**: 147406.

Goze-Bac, C., Latil, S., Lauginie, P., Jourdain, V., Conard, J., Duclaux, L., Rubio, A. and Bernier, P. (2002). Magnetic interactions in carbon nanostructures, *Carbon* **40**: 1825–1842.

Hafner, J. H., Cheung, C. L. and Lieber, C. M. (1999). Growth of nanotubes for probe microscopy tips, *Nature* **398**: 761.

Hamada, N., Sawada, S. and Oshiyama, A. (1992). New one-dimensional conductors: Graphitic microtubules, *Phys. Rev. Lett.* **68**: 1579.1581.

Han, S. W., Yoon, M., Berber, S., Park, N., Osawa, E., Ihm, J. and Tománek, D. (2004). Microscopic mechanism of fullerene fusion, *Phys. Rev. B* **70**: 113402–1–4.

Harneit, W., Meyer, C., Weidinger, A., Suter, D. and Twamley, J. (2002). Architectures for a spin quantum computer based on endohedral fullerenes, *Phys. St. Solidi B* **233**: 453–461.

Hornbaker, D. J., Kahng, S. J., Misra, S., Smith, B. W., Johnson, A. T., Mele, E., Luzzi, D. E. and Yazdani, A. (2002). Mapping the one-dimensional electronic states of nanotube peapod structures, *Science* **295**: 828–831.

Hutchison, J. L., Kiselev, N. A., Krinichnaya, E. P., Krestinin, A. V., Loutfy, R. O., Morawsky, A. P., Muradyan, V. E., Obraztsova, E. D., Sloan, J., Terekhov, S. V. and Zakharov, D. N. (2001). Double-walled carbon nanotubes fabricated by a hydrogen arc discharge method, *Carbon* **39**: 761–770.

Iijima, S. (1991). Helical microtubules of graphitic carbon, *Nature* **354**: 56–58.

Iijima, S. and Ichihashi, T. (1993). Single-shell carbon nanotubes of 1-nm diameter, *Nature* **363**: 603–605.

Ishii, H., Kataura, H., Shiozawa, H., Yoshioka, H., Otsubo, H., Takayama, Y., Miyahara, T., Suzuki, S., Achiba, Y., Nakatake, M., Narimura, T., Higashiguchi, M., Shimada, K., Namatame, H. and Taniguchi, M. (2003). Direct observation of Tomonaga-Luttinger-liquid state in carbon nanotubes at low temperatures, *Nature* **426**: 540–544.

Kane, C. and Mele, E. (1997). Size, Shape, and Low Energy Electronic Structure of Carbon Nanotubes, *Phys. Rev. Lett.* **78**: 1932–1935.

Kane, C. and Mele, E. (2003). Ratio Problem in Single Carbon Nanotube Fluorescence Spectroscopy, *Phys. Rev. Lett.* **90**: 207401–1–4.

Kataura, H., Kumazawa, Y., Maniwa, Y., Umezu, I., Suzuki, S., Ohtsuka, Y. and Achiba, Y. (1999). Optical properties of single-wall carbon nanotubes, *Synthetic Met.* **103**: 2555–2558.

Kataura, H., Maniwa, Y., Kodama, T., Kikuchi, K., Hirahara, K., Suenaga, K., Iijima, S., Suzuki, S., Achiba, Y. and Krätschmer, W. (2001). High-yield fullerene encapsulation in single-wall carbon nanotubes , *Synthetic Met.* **121**: 1195–1196.

Kleinhammes, A., Mao, S.-H., Yang, X.-J., Tang, X.-P., Shimoda, H., Lu, J. P., Zhou, O. and Wu, Y. (2003). Gas adsorption in single-walled carbon nanotubes studied by NMR, *Phys. Rev. B* **68**: 75418–1–6.

Kramberger, C., Pfeiffer, R., Kuzmany, H., Zólyomi, V. and Kürti, J. (2003). Assignment of chiral vectors in carbon nanotubes, *Phys. Rev. B* **68**: 235404.

Krätschmer, W., Lamb, L. D., Fostiropoulos, K. and Huffmann, D. R. (1990). Solid C_{60}: a new form of carbon, *Nature* **347**: 354.

Kresse, G. and Joubert, D. (1999). From ultrasoft pseudopotentials to the projector augmented-wave method, *Phys. Rev. B* **59**: 17581775.

Kroto, H. W., Heath, J. R., O'Brien, S. C., Curl, R. F. and Smalley, R. E. (1985). C_{60}: Buckminsterfullerene, *Nature* **318**: 162–163.

Krupke, R., Hennrich, F., von Lohneysen, H. and Kappes, M. M. (2003). Separation of Metallic from Semiconducting Single-Walled Carbon Nanotubes, *Science* **301**: 344–347.

Kürti, J., Kresse, G. and Kuzmany, H. (1998). First-principles calculations of the radial breathing mode of single-wall carbon nanotubes, *Phys. Rev. B* **58**: R8869–R8872.

Kürti, J., Zólyomi, V., Grüneis, A. and Kuzmany, H. (2002). Double resonant Raman phenomena enhanced by van Hove singularities in single-wall carbon nanotubes, *Phys. Rev. B* **65**: 165433.

Kürti, J., Zólyomi, V., Kertész, M. and Guangyu, S. (2003). The geometry and the radial breathing mode of carbon nanotubes: beyond the ideal behaviour, *New. J. Phys.* **5**: 125.

Kuzmany, H. (1998). *Solid-State Spectroscopy, An Introduction*, Springer Verlag, Berlin.

Kuzmany, H., Plank, W., Hulman, M., Kramberger, C., Grüneis, A., Pichler, T., Peterlik, H., Kataura, H. and Achiba, Y. (2001). Determination of SWCNT diameters from the Raman response of the radial breathing mode, *Eur. Phys. J. B* **22**(3): 307–320.

Liu, X., Pichler, T., Knupfer, M., Golden, M. S., Fink, J., Kataura, H., Achiba, Y., Hirahara, K. and Iijima, S. (2002). Filling factors, structural, and electronic properties of C_{60} molecules in single-wall carbon nanotubes, *Phys. Rev. B* **65**: 045419–1–6.

Marques, M. A. L., d'Avezac, M. and Mauri, F. (2006). Magnetic response of carbon nanotubes from ab initio calculations, *Phys. Rev. B* **73**: 125433–1–6.

Maultzsch, J., Pomraenke, R., Reich, S., Chang, E., Prezzi, D., Ruini, A., Molinari, E., Strano, M. S., Thomsen, C. and Lienau, C. (2005). Exciton binding energies in carbon nanotubes from two-photon photoluminescence, *Phys. Rev. B* **72**: 241402.

Meese, J. (1979). *Neutron Transmutation Doping of Semiconductors*, Plenum Press, NY.

Melle-Franco, M., Kuzmany, H. and Zerbetto, F. (2003). Mechanical interaction in all-carbon peapods, *J. Phys. Chem. B* **109**: 6986–6990.

Mintmire, J. and White, C. (1998). Universal Density of States for Carbon Nanotubes, *Phys. Rev. Lett.* **81**: 2506.

Monthioux, M. and Kuznetsov, V. L. (2006). Who should be given the credit for the discovery of carbon nanotubes?, *Carbon* **44**: 1621–1624.

Moriya, T. (1963). The Effect of Electron-Electron Interaction on the Nuclear Spin Relaxation in Metals, *J. Phys. Soc. Jpn.* **18**: 516.

Novoselov, K. S., Geim, A. K., Morozov, S. V., Jiang, D., Zhang, Y., Dubonos, S. V., Grigorieva, I. V. and Firsov, A. A. (2004). Electric field effect in atomically thin carbon films, *Science* **306**: 666–669.

Obraztsov, A. N., Pavlovsky, I., Volkov, A. P., Obraztsova, E. D., Chuvilin, A. L. and Kuznetsov, V. L. (2000). Aligned carbon nanotube films for cold cathode applications, *J. Vac. Sci. Techn. B* **18**: 1059–1063.

Okada, S. and Oshiyama, A. (2003). Curvature-Induced Metallization of Double-Walled Semiconducting Zigzag Carbon Nanotubes, *Phys. Rev. Lett.* **91**: 216801–1–4.

Otani, M., Okada, S. and Oshiyama, A. (2003). Energetics and electronic structures of one-dimensional fullerene chains encapsulated in zigzag nanotubes, *Phys. Rev. B* **68**: 125424–1–8.

Perebeinos, V., Tersoff, J. and Avouris, P. (2004). Scaling of Excitons in Carbon Nanotubes, *Phys. Phys. Lett.* **92**: 257402–1–4.

Pfeiffer, R., Kuzmany, H., Kramberger, C., Schaman, C., Pichler, T., Kataura, H., Achiba, Y., Kürti, J. and Zólyomi, V. (2003). Unusual High Degree of Unperturbed Environment in the Interior of Single-Wall Carbon Nanotubes, *Phys. Rev. Lett.* **90**: 225501–1–4.

Popov, V. N. (2004). Curvature effects on the structural, electronic and optical properties of isolated single-walled carbon nanotubes within a symmetry-adapted non-orthogonal tight-binding model, *New J. Phys.* **6**: 17.

Rauf, H., Pichler, T., Knupfer, M., Fink, J. and Kataura, H. (2004). Transition from a Tomonaga-Luttinger Liquid to a Fermi Liquid in Potassium-Intercalated Bundles of Single-Wall Carbon Nanotubes, *Phys. Rev. Lett.* **93**: 096805–1–4.

Reich, S., Thomsen, C. and Maultzsch, J. (2004). *Carbon Nanotubes*, Wiley-VCH, Weinheim.

Ren, W., Li, F., Chen, J., Bai, S. and Cheng, H.-M. (2002). Morphology, diameter distribution and Raman scattering measurements of double-walled carbon nanotubes synthesized by catalytic decomposition of methane, *Chem. Phys. Lett.* **359**: 196–202.

Rochefort, A. (2003). Electronic and transport properties of carbon nanotube peapods, *Appl. Magn. Reson.* **67**: 11540117.

Rümmeli, M. H., Löffler, M., Kramberger, C., Simon, F., Fülöp, F., Jost, O., Schönfelder, R., Grüneis, R., Gemming, T., Pompe, W., Büchner, B. and Pichler, T. (2007). Isotope-Engineered Single-Wall Carbon Nanotubes; A Key Material for Magnetic Studies, *J. Phys. Chem. C* **111**: 4094.

Saito, R., Dresselhaus, G. and Dresselhaus, M. (1998). *Physical Properties of Carbon Nanotubes*, Imperial College Press.

Shimoda, H., Gao, B., Tang, X. P., Kleinhammes, A., Fleming, L., Wu, Y. and Zhou, O. (2002). Lithium Intercalation into Opened Single-Wall Carbon Nanotubes: Storage Capacity and Electronic Properties, *Phys. Rev. Lett.* **88**: 15502.

Shlimak, I. (2004). Isotopically engineered silicon nanostructures in quantum computation and communication, *HAIT J. Sci. Eng.* **1**: 196–206.

Simon, F., Kramberger, C., Pfeiffer, R., Kuzmany, H., Zólyomi, V., Kürti, J., Singer, P. M. and Alloul, H. (2005). Isotope Engineering of Carbon Nanotube Systems, *Phys. Rev. Lett.* **95**: 017401.

Simon, F., Kukovecz, A., Kramberger, C., Pfeiffer, R., Hasi, F., Kuzmany, H. and Kataura, H. (2005). Diameter selective characterization of single-wall carbon nanotubes, *Phys. Rev. B* **71**: 100–122.

Simon, F., Peterlik, H., Pfeiffer, R. and Kuzmany, H. (2007). Fullerene release from the inside of carbon nanotubes: A possible route toward drug delivery, *Chem. Phys. Lett.* **445**: 288–292.

Simon, F., Pfeiffer, R., Kramberger, C., Holzweber, M. and Kuzmany, H. (2005). *The Raman response of double wall carbon nanotubes in "Applied Physics of Carbon Nanotubes", S. V. Rotkin and S. Subramoney eds.*, Springer New York, pp. 203–224.

Singer, P. M., Wzietek, P., Alloul, H., Simon, F. and Kuzmany, H. (2005). NMR Evidence for Gapped Spin Excitations in Metallic Carbon Nanotubes, *Phys. Rev. Lett.* **95**: 236403–1–4.

Slichter, C. P. (1989). *Principles of Magnetic Resonance*, 3rd ed. 1996 edn, Spinger-Verlag, New York.

Smith, B. W. and Luzzi, D. (2000). Formation mechanism of fullerene peapods and coaxial tubes: a path to large scale synthesis, *Chem. Phys. Lett.* **321**: 169–174.

Smith, B. W., Monthioux, M. and Luzzi, D. (1999). Carbon nanotube encapsulated fullerenes: a unique class of hybrid materials, *Chem. Phys. Lett.* **315**: 31–36.

Smith, B. W., Monthioux, M. and Luzzi, D. E. (1998). Encapsulated C_{60} in carbon nanotubes, *Nature* **396**: 323–324.

Spataru, C. D., Ismail-Beigi, S., Benedict, L. X. and Louie, S. G. (2004). Excitonic Effects and Optical Spectra of Single-Walled Carbon Nanotubes, *Phys. Rev. Lett.* **92**: 077402–1–4.

Stone, A. J. and Wales, D. J. (1986). Theoretical-studies of icosahedral C_{60} and some related species, *Chem. Phys. Lett.* **128**: 501–503.

Tang, X.-P., Kleinhammes, A., Shimoda, H., Fleming, L., Bennoune, K. Y., Sinha, S., Bower, C., Zhou, O. and Wu, Y. (2000). Electronic Structures of Single-Walled Carbon Nanotubes Determined by NMR, *Science* **288**: 492.

Tans, S. J., Devoret, M. H., Dai, H., Thess, A., Smalley, R. E., Geerligs, L. J. and Dekker, C. (1997). Individual single-wall carbon nanotubes as quantum wires, *Nature* **386**: 474 – 477.

Telg, H., Maultzsch, J., Reich, S., Hennrich, F. and Thomsen, C. (2004). Chirality Distribution and Transition Energies of Carbon Nanotubes, *Phys. Rev. Lett.* **93**: 177401.

Thomsen, C. and Reich, S. (2000). Double Resonant Raman Scattering in Graphite, *Phys. Rev. Lett.* **85**: 5214–5217.

Wang, F., Dukovic, G., , Brus, L. E. and Heinz, T. F. (2005). The Optical Resonances in Carbon Nanotubes Arise from Excitons, *Science* **308**: 838–841.

Wildör, J. W. G., Venema, L. C., Rinzler, A. G., Smalley, R. E. and Dekker, C. (1998). Electronic structure of atomically resolved carbon nanotubes, *Nature* **391**: 59–62.

Yue, G. Z., Qiu, Q., Gao, B., Cheng, Y., Zhang, J., Shimoda, H., Chang, S., Lu, J. P. and Zhou, O. (2002). Generation of continuous and pulsed diagnostic imaging x-ray radiation using a carbon-nanotube-based field-emission cathode, *Appl. Phys. Lett.* **81**: 355–368.

Zhao, Y., Yakobson, B. I. and Smalley, R. E. (2002). Dynamic Topology of Fullerene Coalescence, *Phys. Rev. Lett.* **88**: 185501–1–4.

Zheng, M., Jagota, A., Strano, M. S., Santos, A. P., Barone, P., Chou, S. G., Diner, G., B. A. Dresselhaus, M. S., McLean, R. S., Onoa, G. B., Samsonidze, G. G., Semke, E. D., Usrey, M. and Walls, D. J. (2003). 2003, *Science* **302**: 1545–1548.

Zólyomi, V., Koltai, J., Rusznyák, A., Kürti, J., Gali, A., Simon, F., Kuzmany, H., Szabados, A. and Surján, P. R. (2008). Intershell interaction in double walled carbon nanotubes: Charge transfer and orbital mixing, *Phys. Rev. B* **77**: 245403–1–10.

Zólyomi, V. and Kürti, J. (2004). First-principles calculations for the electronic band structures of small diameter single-wall carbon nanotubes, *Phys. Rev. B* **70**: 085403–1–8.

Zólyomi, V., Kürti, J., Grüneis, A. and Kuzmany, H. (2003). Origin of the Fine Structure of the Raman D Band in Single-Wall Carbon Nanotubes, *Phys. Rev. Lett.* **90**: 157401.

Zólyomi, V., Simon, F., Rusznyák, A., Pfeiffer, R., Peterlik, H., Kuzmany, H. and Kürti, J. (2007). Inhomogeneity of ^{13}C isotope distribution in isotope engineered carbon nanotubes: Experiment and theory, *Phys. Rev. B* **75**: 195419–1–8.